Available online at www.sciencedirect.com

ScienceDirect

Procedia Structural Integrity 42 (2022) 1736–1743

Structural Integrity Procedia

www.elsevier.com/locate/procedia

23 European Conference on Fracture – ECF23

Numerical analysis of ballistic impact through FE and SPH methods

Yağmur Göçmen[a], Hande Vural[a], Can Erdoğan[a], Tuncay Yalçinkaya[a,*]

[a]*Department of Aerospace Engineering, Middle East Technical University, 06800 Ankara , Turkey*

Abstract

In the defense and aerospace industries, structures are designed to resist ballistic impact loads. Experimental analysis of ballistic impact has been conducted successfully for many years, and alternatively, numerical techniques have been employed to reduce the experimental cost. In this study, the ballistic impact of metallic materials is addressed with both finite element (FE) and smoothed particle hydrodynamics (SPH) methods. A single-shot ballistic impact model consisting of a deformable plate and a rigid projectile is developed. These two methods are compared using Johnson-Cook (JC) and Modified Mohr-Coulomb (MMC) damage models. Lode parameter dependent MMC damage criterion is implemented in the user-defined field (VUSDFLD) for damage analysis. Various numerical setups with varying target thickness, impact velocity, projectile nose shape and impact angle of the projectile, are generated. The damage response of the plate target according to the impact angle and the nose shape and the effect of ballistic impact parameters on the residual velocity is discussed in detail. The results are compared with the experimental results from the literature. FE method is found to be more consistent than SPH method in the prediction residual velocity. MMC damage model is better in agreement with experimental data than JC damage model. A linear decrease in residual velocity is observed with increasing thickness of target except the JC model used with FE method. Moreover, blunt projectiles are more sensitive to change in the impact angle than hemispherical and ogival projectiles. Increase in impact angle cause a reduction in residual velocity for all three projectile.

Keywords: Ballistic impact; Ductile damage; FEM; SPH

1. Introduction

The ballistic impact is a process in which materials are exposed to high strain rate loading. Many structures produced in the aerospace and defense industries are expected to be resistant to impact loads, e.g., bullet impact on military vehicles and bird strikes in aviation. Failure analyses of materials may be performed by making ballistic impact tests to assist the design process. The ballistic impact testing set-up consists of a projectile and a target. Target plates are made of high-strength metals such as aluminum and steel alloys. By investigating the behavior of the target against the impact load, stronger and more resilient structures can be designed and manufactured.

* Yalçinkaya T. Tel.: +90-312-210-4258 ; fax: +90-312-210-4250.
E-mail address: yalcinka@metu.edu.tr

10.1016/j.prostr.2022.12.220

The fracture behavior of the target is highly dependent on several variables such as velocity, nose shape of the projectile, the thickness of the target plate angle, and the angle of the impact. Since the ballistic impact is a highly parameter-dependent process, experiments are required to determine the ballistic limit of the materials.

As an alternative to experiments, numerical approaches are shown to be efficient in predicting the results. Finite element (FE) method has been used successfully for the numerical simulation of ballistic impact (see e.g. Elek et al. (2016), Fras et al. (2019)). However, simulations of failure under large deformations with the FE method are prone to high mesh dependencies and mesh distortion problems. To overcome mesh-related problems, meshless simulation methods have been proposed, such as smoothed particle hydrodynamics (SPH). SPH is a particle-based method in which smoothed field variables are calculated by particle interpolation. The numerical model geometry is defined by these particles, which have a mass, velocity, and position. SPH method is a good alternative for the simulations of impact to overcoming of FE method. However, essential boundary conditions cannot be satisfied in SPH, and it has a higher computational cost. In Xiao et al. (2017) and Rodriguez-Millan et al. (2018), SPH method is utilized to study ballistic impact with different target thicknesses and projectile nose shapes.

Ballistic impact on metal targets results in ductile fracture. Simulation of ductile failure with numerical method usually involves phenomenological fracture models that predict the evolution of damage based on several factors such as plastic strain, stress, temperature, etc. For example, Holmen et al. (2015, 2016) used the stress-dependent Cockcroft-Latham (CL) (Cockcroft (1968)) failure criterion to examine the ballistic resistance of using steel and aluminum alloys. Johnson-Cook (JC) (Johnson and Cook (1985)) is one of the widely used damage models that include effects of stress triaxiality, strain rate, and temperature. In literature, there are many implementations of this model in ballistic impact simulations, and results are in reasonable agreement with experiments (see e.g. Rai et al. (2021); Dey et al. (2004)). However, the JC criterion does not include the Lode parameter related to shear stress. Because the ballistic impact has a shear dominant character, the Lode parameter may be included in the damage model. The Modified Mohr-Coulomb (MMC) (Bai and Wierzbicki (2010)) damage model is a strain rate-independent model that includes stress triaxiality and Lode parameters. Since ballistic impact tests are strain rate-dependent, in the current work, strain rate effects in JC damage model are implemented in MMC model following the work in Xiao et al. (2019).

In the literature, many investigations are concerned with the effects of parameters in ballistic impacts. Roth et al. (2020) and Mohammad et al. (2020) studied oblique and perpendicular impact with blunt, hemispherical, and conical projectile nose shapes and validated their results with experiments. Both studies found different failure mechanisms and residual velocities for different projectile nose shapes and oblique angles depending on the set-up configuration. The residual velocity results for both papers varied for the hemispherical and conical nose shapes. In one of the studies conical nose shape was the most sensitive to impact angle. However, in the second paper blunt nose shape was observed to be most sensitive among the nose shapes. Furthermore, the influence of thickness variations in ballistic impacts is studied in Vershinin (2015); Shrivastava et al. (2020); Edwards et al. (2022). It is observed that with an increase in thickness, the minimum impact velocity required to penetrate the target increases as well. By increasing the thickness of the target, more types of failure mechanisms are observed to occur simultaneously and an increase in the size of the cracked pieces are observed.

The aim of this study is to examine the effects of projectile nose shape, the thickness of the target plate, and the angle of the impact on ballistic impact. This study uses the JC plasticity model to define yield stress. JC and strain rate-dependent MMC models are used for failure predictions. The MMC damage model is implemented in a user-defined field (VUSDFLD), and for the JC model, the built-in framework is used in Abaqus. Plasticity and failure model parameters are adopted from Wang et al. (2020). Using these two damage criteria, ballistic impact simulations are performed using FE and SPH methods in Abaqus. Ballistic impact simulations are conducted for 2024-T351 aluminum alloy target with blunt, hemispherical, and ogival nose shapes at 3 mm, 6 mm, and 9.94 mm thicknesses, with an initial velocity of 100 to 400 m/s. The results from the numerical simulations are compared and discussed with the experimental data in Wang et al. (2020).

2. Methods

2.1. Material

In this study, the target material is chosen as aluminium alloy 2024-T351, a ductile metal that is commonly used in ballistic impact tests in the aerospace industry. Ballistic impact experimental data, plasticity, and damage model parameters are taken from Wang et al. (2020). Classical J_2 plasticity framework is used to define the metal plasticity, and yield stress is described by JC plasticity, which is a particular type of isotropic hardening, and it is shown as follows,

$$\sigma_y = (A + B\varepsilon_{eq}^n)(1 + C \ln \dot{\varepsilon_{eq}}^*)(1 - T^{*m}) \tag{1}$$

A, B, C, m and n are material constants, and ε_{eq} is the equivalent plastic strain. For the strain hardenining part in the yield stress, the equation used in the aforementioned study is simplified to the form shown above. Strain rate ratio is expressed as $\dot{\varepsilon_{eq}}^* = \dot{\varepsilon_{eq}}/\dot{\varepsilon_0}$ in which $\dot{\varepsilon_{eq}}$ is present strain rate and $\dot{\varepsilon_0}$ is the reference strain rate. Homologous temperature is $T^* = (T - T_0)/(T_m - T_0)$ where T_0 is the room temperature, T_m is the melting temperature. Young's modulus, Poisson's ratio and density of aluminum alloy 2024-T351 are 72 GPa, 0.3 and 2.77 g/cm^3 respectively.

Table 1: Material parameters of aluminum alloy 2024-T351.

E(GPa)	ν	$\rho(g/cm^3)$	A(MPa)	B(MPa)	n	C	m	$\dot{\varepsilon_0}^*$(1/s)	T_0 (K)	T_m (K)
72	0.3	2.77	235.7	377.5	0.1752	0.0146	1.7	8.336×10^{-4}	293	775

Stress state is expressed with stress triaxiality, T, and Lode angle parameter, $\bar{\theta}$. These dimensionless parameters are shown as follows,

$$T = \frac{\sigma_h}{\sigma_{eq}}, \bar{\theta} = 1 - \frac{6\theta_L}{\pi} \quad \text{where} \quad \theta_L = \frac{1}{3}\arccos\left(\frac{J_3}{2}\left(\frac{3}{J_2}\right)^{3/2}\right) \tag{2}$$

where I_1 is first stress invariant,the hydrostatic stress is $\sigma_h = I_1/3$, J_2 is the second stress invariant and J_3 is the third deviatoric stress invariant.

2.2. Ductile Damage Criteria

In the context of this study, JC and MMC ductile damage criteria are compared for ballistic impact failure analysis. JC is a strain rate and temperature-dependent ductile fracture criterion. Although the temperature effect is included in the plasticity model, only the strain rate effect is included in the damage model. Strain rate-dependent JC formulation is defined as follows,

$$\varepsilon_f = [D_1 + D_2 exp(D_3\eta)](1 + D_4 \ln \dot{\varepsilon_{eq}}^*) \tag{3}$$

where D_1, D_2, D_3, D_4 and D_5 are the JC fracture criterion constants, and these values are shown in Table 2.

Since the JC criterion does not contain the Lode parameter, it is not sufficient for the estimation of failure in shear dominant models. For this reason, the Lode parameter and strain rate dependent MMC model is used in the failure analysis. The model is formulated as,

$$\varepsilon_f = \left\{\frac{\hat{A}}{\hat{C}_2}\left[\hat{C}_3 + \frac{\sqrt{3}}{2-\sqrt{3}}\left(1-\hat{C}_3\right)\left(\sec\left(\frac{\bar{\theta}\pi}{6}\right) - 1\right)\right]\right\} \times \left[\sqrt{\frac{1+\hat{C}_1^2}{3}}\cos\left(\frac{\bar{\theta}\pi}{6}\right) + \hat{C}_1\left(T + \frac{1}{3}\sin\left(\frac{\bar{\theta}\pi}{6}\right)\right)\right]^{-1/n} \times (1 + D_4 \ln \dot{\varepsilon_{eq}}^*) \tag{4}$$

where $\hat{C}_1, \hat{C}_2, \hat{C}_3, \hat{C}_4$, K and n are the MMC fracture criterion constants which are given in Table 2.

Table 2: JC and MMC fracture criteria constants for aluminum alloy 2024-T351.

D_1	D_2	D_3	D_4	
0.034	0.664	-1.5	0.011	
K(MPa)	$\hat{C}_1$	$\hat{C}_2$(MPa)	$\hat{C}_3$	n
678.7	0.104	335.6	1.036	0.138

Damage, D, is evaluated as follows:

$$D = \int_0^{\bar{\varepsilon}_p} \frac{d\bar{\varepsilon}_p}{\varepsilon_f(\bar{\theta}, T)} \tag{5}$$

Damage value starts as zero and a material point is considered to be completely failed at $D = 1$.

2.3. Numerical Modelling

In the present study, MMC is implemented with a user-defined field subroutine (VUSDFLD). These damage criteria are employed for FE and SPH simulations of ballistic impact in Abaqus/Explicit. Ballistic impact consists of a target and a projectile. In the numerical model, the projectile is modeled as a rigid body, and the target is a deformable body. Three projectile nose shapes are used, named as blunt, hemispherical, and ogival, with a mass of 50 g and a diameter of 12.66 mm. In Fig. 1, the geometrical shapes of the projectiles and the target are presented. The thickness of the target is assigned values of 3 mm, 6 mm, and 9.94 mm, where the target has a diameter of 116 mm, and the investigated impact angles are 0°, 15°, 30°, 45°, and 60°. The impact angle, alpha, is shown in Fig. 1.

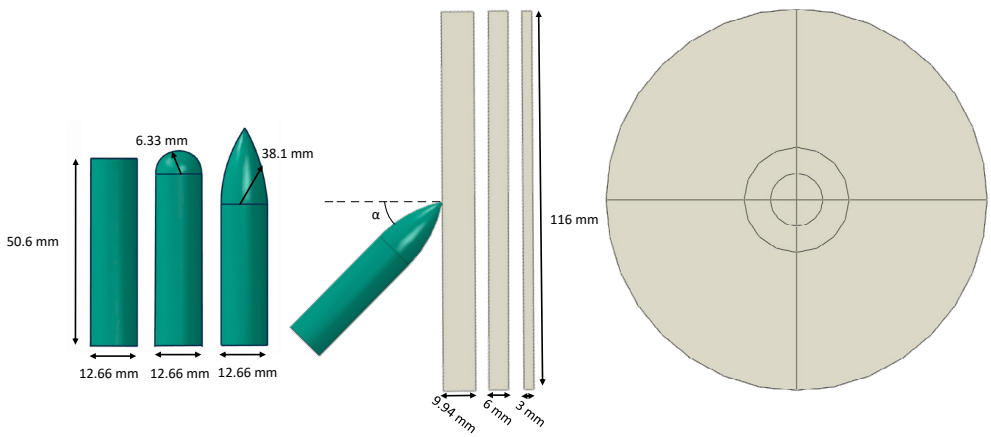

Fig. 1: Geometry of the projectiles and targets

Only the quarter portion of the target plate is modeled in FEM using the symmetry boundary conditions. For the oblique impact simulations, half of the target plate is simulated to accurately represent the impact. The curved outer face of the target is completely constrained, and for surfaces in the plane of symmetry, only the displacement perpendicular to the plane is limited. The contact property between the projectile and the target is adopted as ”hard” contact and frictionless. The surface of the bullet and the penetration zone of the target are selected in the contact algorithm.

The influence of element number through the thickness on the residual velocity is checked, and observations showed that the ogival model is relatively inelastic in this regard, whereas both hemispherical and blunt showed increasing residual velocities with a higher number of elements through the thickness. However, considering the fact

that this difference is not significant and the length of the solution time, a model with 33 elements through the thickness is chosen. Moreover, the target is meshed with hexahedral linear elements with reduced integration (C3D8R). In FE models, the penetration zone is divided into partitions, and this zone is discretized with smaller elements than the outside of the target. In the SPH method, if the model is partitioned, the separation occurs at the partition boundaries during impact. Therefore, in SPH method models, the size of the elements is decreased with a biased mesh from the edges to the center without creating a partition in the model.

3. Results and Discussion

A comparison of FE and SPH methods with JC and MMC damage models for hemispherical,blunt and ogival projectiles are portrayed in Fig. 2a, Fig. 2b and Fig. 2c, respectively. The relation between initial and residual velocities is explored for a combination of different methodologies and material models for the three nose shapes. The initial velocity of the projectile is between 100 m/s to 400 m/s. The minimum initial velocity required to achieve a non-zero residual velocity is highest for the FE-JC model for all three nose shapes. In each of the three cases, different models coincided with experimental data. Furthermore, in all three nose shapes, it is observed that the FE-MMC model has the best and most consistent agreement with experiments. At higher initial velocities for all three nose shapes, the various models seem to converge toward experimental results.

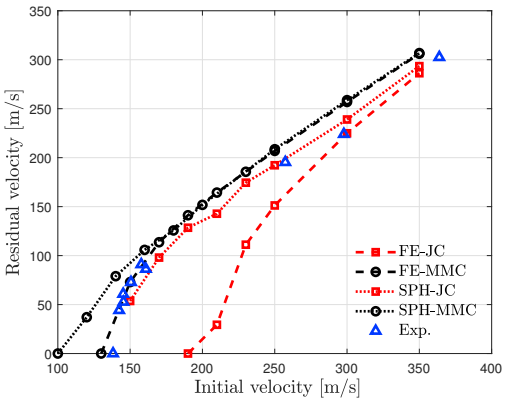

(a) Blunt projectile

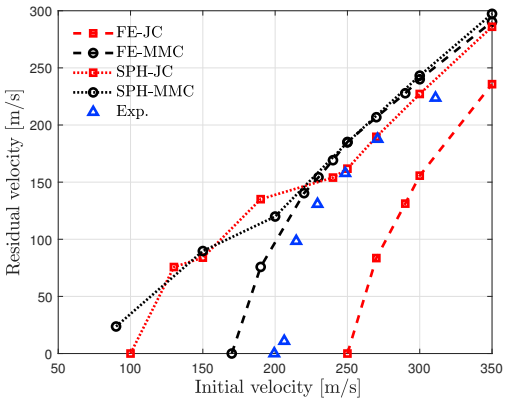

(b) Hemispherical projectile

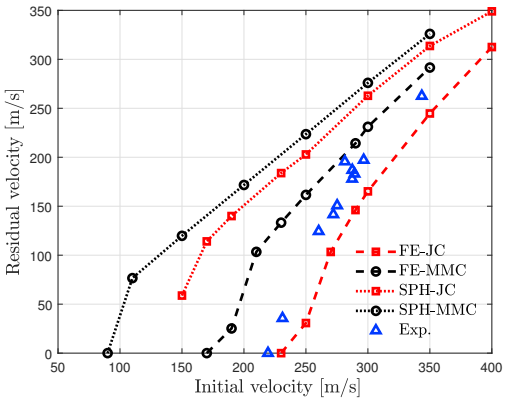

(c) Ogival projectile

Fig. 2: Initial vs. residual velocity curves of FE-JC, FE-MMC, SPH-JC, SPH-MMC models for blunt, hemispherical and ogival projectile. t = 9.94 mm. Experimental data are taken from Wang et al. (2020).

Target is impacted by a hemispherical projectile at target thicknesses of 3 mm, 6 mm, and 9.94 mm. Simulations are conducted in three thicknesses at velocities from 50 m/s to 350 m/s. In Fig. 3a, the effect of varying thickness of the target plate on residual velocity for 250 m/s initial velocity is depicted. The minimum initial velocity required for non-zero residual velocity increases with increasing thickness. For example, in the results of FE-MMC, minimum required velocity to penetrate the target should be more than 170 m/s at 9.94 mm thickness, while this value needs to be more than 110 m/s at 6 mm thickness and more than 70 m/s at 3 mm thickness. With increasing thickness, the results of the models seem to diverge from each other. Especially FE-JC deviates from the other models at higher thicknesses, and the projectile failed to penetrate the target with this model.

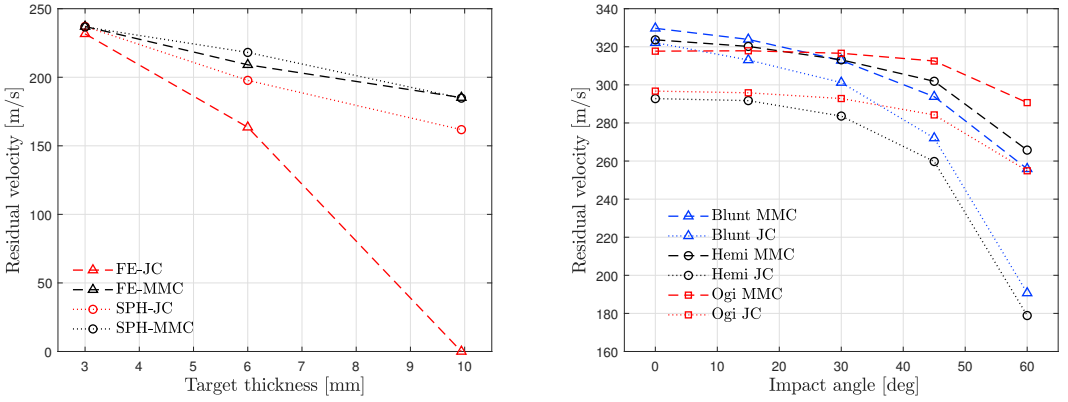

Fig. 3: (a) Target thickness vs. residual velocity curves of hemispherical projectile for FE-JC, FE-MMC, SPH-JC, SPH-MMC models at 250 m/s initial velocity with 3 mm, 6 mm, and 9.94 mm target thicknesses. (b) Impact angle vs. residual velocity curves of blunt, hemispherical, and ogival projectile for FE-JC and FE-MMC models at 350 m/s initial velocity with 6 mm target thickness.

The target is impacted at 0°, 15°, 30°, 45°, and 60° obliquity at the initial velocity of 350 m/s and the comparison is described in Fig. 3b. This comparison is made for three projectile nose shapes using JC and MMC damage models with FE method. Fig. 3b shows that as obliquity increases, residual velocity decreases. In the case of 0°,15°, and 30° obliquity, hemispherical, and ogival nose-shaped projectiles, the residual velocity change is insignificant. However, for blunt-nosed projectiles, change in residual velocity is sensitive to obliquity. From 45° to 60° obliquity, there is a significant drop in residual velocity for blunt and hemispherical projectile in JC model. For blunt projectile, the decrease in residual velocity for JC and MMC models are approximately 30% and 13%, respectively. Similar behavior is observed for hemispherical projectiles, where JC and MMC decrease in the residual velocity is 31% and 12%, respectively. However, ogival projectile exhibited a 10% and 7% decrease in residual velocity for JC and MMC cases, respectively. For JC models in all three cases, the residual velocities are much lower for all angles than their respective MMC counterparts.

For different nose shapes, the failure mechanism shows different behaviors and the simulations results are shown in Fig. 4. The blunt projectile perforates the target by shear plugging, which is a failure mechanism where a plug is separated from the target and creates a hole. At the higher obliquity of the target, the formed plug starts to crack into small pieces. Furthermore, hemispherical projectiles show shear plugging and petaling failure mechanisms depending on the simulation setup's configuration. Petaling is a phenomenon that occurs at high strain rates typically associated with impact, where metal deforms around the point of impact into thin sheets resembling flower petals. At 0° and 15°, obliquity plug formation and fragmentation occur. However, as obliquity increases, at 45° and 60° obliquity, the number of cracks increases as well as the size of the hole.

Ogival projectiles failure mechanism is shown in Fig. 5 where the target is impacted at 0°, 15°, 30°, 45°, and 60° obliquity. With the initial velocity of 350 m/s, simulations show that in ogival nose shape, the failure mechanism of the target plate is ductile hole enlargement. In the JC-FE case, at higher obliquity, petal forming starts to occur. However, for the MMC-FE case, small petals are observed in lower obliquity, and as the obliquity is increased, cracks of petals are observed. Lastly, a similar trend is observed in the MMC-SPH case as in the JC-FE case. It can be concluded that

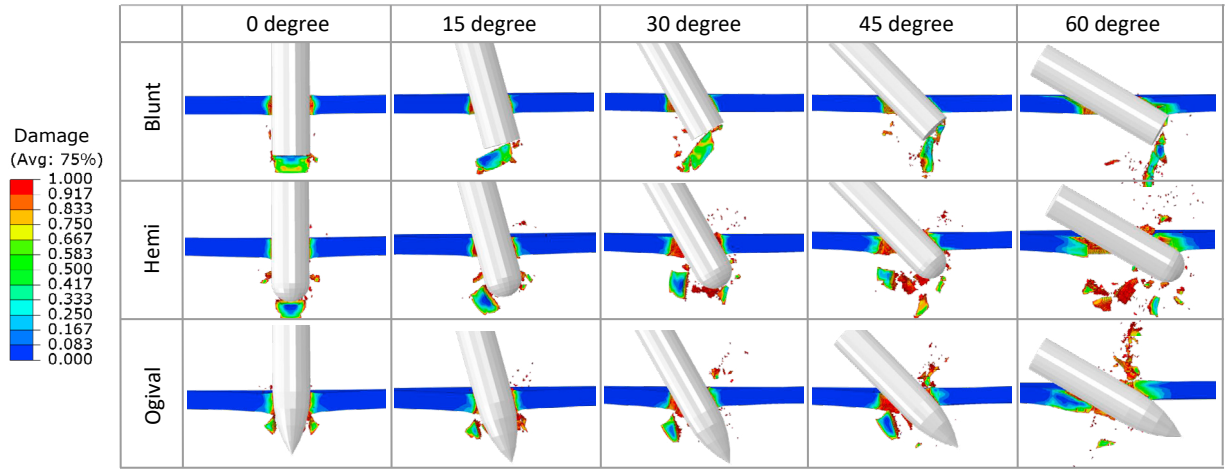

Fig. 4: Failure mechanisms of blunt, hemispherical, and ogival projectile at 350 m/s initial velocity with 6 mm thickness for 0°, 15°, 30°, 45°, and 60° obliquity.

for all cases with the increase in obliquity size of the ductile hole enlargement and the size of the formed petals are increased.

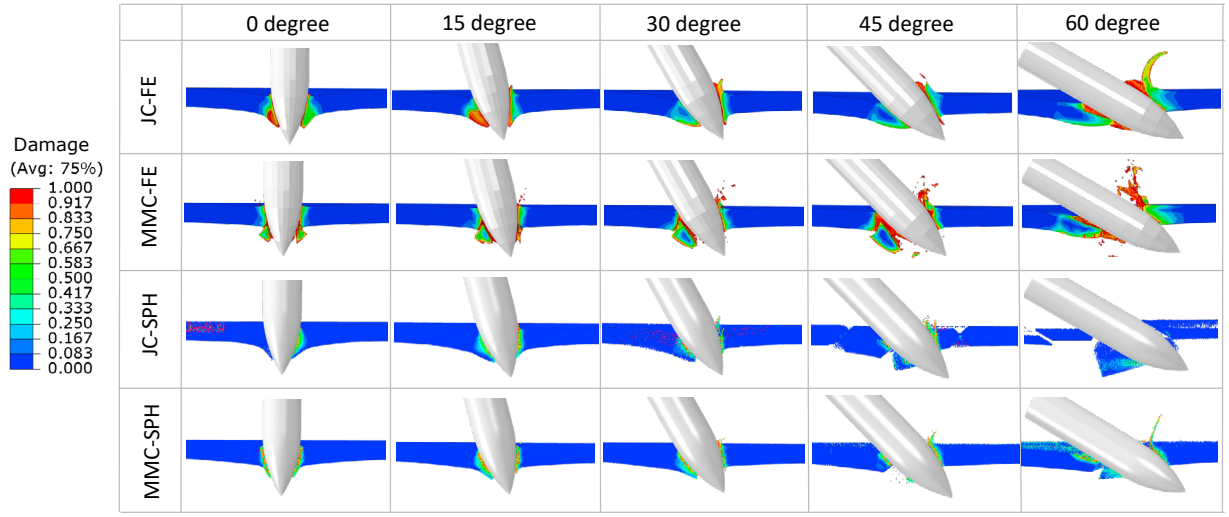

Fig. 5: Failure mechanisms of 6 mm thickness ogival projectile at 350 m/s initial velocity with FE-JC, FE-MMC, SPH-JC, SPH-MMC for 0°, 15°, 30°, 45°, and 60° obliquity.

4. Conclusion

This study investigates the effect of projectile nose shapes, target thickness and impact angle in ballistic impact using numerical simulations. The damage model and material parameters are taken from literature as well as experimental data. FE and SPH methods are compared using JC and MMC damage models. It is observed that for FE method, MMC and JC models have significantly varying results, whereas the MMC model is in better agreement with experiments. However, in SPH method, JC and MMC models are in relatively better agreement for blunt and

hemispherical projectile. SPH method results in higher residual velocity values compared to experimental data for ogival projectile. Moreover, results show that decreasing the thickness of the target plate resulted in a linear increase of residual velocity except in JC model. Regarding the oblique impact simulations, increasing the obliquity of the target plate resulted in increased hole size and an increase in the separation of petals from the target. Blunt projectile has significant velocity changes in all impact angle changes, while other two projectiles do not change much in velocity at low angles. While the FE method is consistent in most cases, the SPH method overpredicts the residual velocity results at initial velocities less than 200 m/s for except blunt shaped projectiles. In addition, some SPH simulations have difficulty showing the failure mechanism of the target. In future studies, it is planned to develop a coupled SPH-FE model to extend the modeling approaches. Moreover, predictions can be improved by implementing other damage models, including coupled damage frameworks.

References

Bai, Y., Wierzbicki, T., 2010. Application of extended mohr-coulomb criterion to ductile fracture. International Journal of Fracture 161, 1–20.

Cockcroft, M., 1968. Ductility and workability of metals. J. of Metals. 96, 2444.

Dey, S., Børvik, T., Hopperstad, O., Leinum, J., Langseth, M., 2004. The effect of target strength on the perforation of steel plates using three different projectile nose shapes, pp. 1005–1038. Eighth International Symposium on Plasticity and Impact Mechanics (IMPLAST 2003).

Edwards, N.J., Cimpoeru, S.J., Herzig, .N., Ruan, D., 2022. Ballistic impact of flat-ended projectiles against 2024-T351 plate: Experiments and modeling. Journal of Aerospace Engineering 35, 04021124.

Elek, P.M., Jaramaz, S.S., Micković, D.M., Miloradović, N.M., 2016. Experimental and numerical investigation of perforation of thin steel plates by deformable steel penetrators. Thin-Walled Structures 102, 58–67.

Fras, T., Roth, C.C., Mohr, D., 2019. Dynamic perforation of ultra-hard high-strength armor steel: Impact experiments and modeling. International Journal of Impact Engineering 131, 256–271.

Holmen, J.K., Hopperstad, O.S., Børvik, T., 2015. Low-velocity impact on multi-layered dual-phase steel plates. International Journal of Impact Engineering 78, 161–177.

Holmen, J.K., Johnsen, J., Hopperstad, O.S., Børvik, T., 2016. Influence of fragmentation on the capacity of aluminum alloy plates subjected to ballistic impact. European Journal of Mechanics, A/Solids 55, 221–233.

Johnson, G.R., Cook, W.H., 1985. Fracture characteristics of three metals subjected to various strains, strain rates, temperatures and pressures. Engineering Fracture Mechanics 21, 31–48.

Mohammad, Z., Gupta, P.K., Baqi, A., 2020. Experimental and numerical investigations on the behavior of thin metallic plate targets subjected to ballistic impact. International Journal of Impact Engineering 146, 103717.

Rai, R., Kumar, G., Dagar, S., Somashekar, V., Mboreha, C.A., Modi, P., 2021. Numerical simulation of ballistic impact on aluminium 5083-H116 plate with johnson cook plasticity model, Elsevier Ltd. pp. 10619–10627. International Conference on Technological Advancements in Materials Science and Manufacturing.

Rodriguez-Millan, M., Garcia-Gonzalez, D., Rusinek, A., Abed, F., Arias, A., 2018. Perforation mechanics of 2024 aluminium protective plates subjected to impact by different nose shapes of projectiles. Thin-Walled Structures 123, 1–10.

Roth, C.C., Fras, T., Mohr, D., 2020. Dynamic perforation of lightweight armor: Temperature-dependent plasticity and fracture of aluminum 7020-T6. Mechanics of Materials 149, 103537.

Shrivastava, S., Tiwari, G., Iqbal, M., Gupta, P., 2020. The ballistic performance of thin aluminium plates against blunt-nosed projectile. Materials Today: Proceedings 21, 1763–1771. International Symposium on Functional Materials (ISFM-2018): Energy and Biomedical Applications.

Vershinin, V.V., 2015. Validation of metal plasticity and fracture models through numerical simulation of high velocity perforation. International Journal of Solids and Structures 67-68, 127–138.

Wang, Y., Chen, X., Xiao, X., Vershinin, V.V., Ge, R., Li, D., 2020. Effect of lode angle incorporation into a fracture criterion in predicting the ballistic resistance of 2024-T351 aluminum alloy plates struck by cylindrical projectiles with different nose shapes. International Journal of Impact Engineering 139, 103498.

Xiao, X., Pan, H., Bai, Y., Lou, Y., Chen, L., 2019. Application of the modified mohr–coulomb fracture criterion in predicting the ballistic resistance of 2024-T351 aluminum alloy plates impacted by blunt projectiles. International Journal of Impact Engineering 123, 26–37.

Xiao, Y., Dong, H., Zhou, J., Wang, J., 2017. Studying normal perforation of monolithic and layered steel targets by conical projectiles with sph simulation and analytical method. Engineering Analysis with Boundary Elements 75, 12–20.